Integrated Photovoltaic and Dynamic Voltage Restorer System Configuration

Abdul Mannan Rauf and Vinod Khadkikar, *Member, IEEE*

***Abstract*—This paper presents a new system configuration for integrating a grid-connected photovoltaic (PV) system together with a self-supported dynamic voltage restorer (DVR). The proposed system termed as a "six-port converter," consists of nine semiconductor switches in total. The proposed configuration retains all the essential features of normal PV and DVR systems while reducing the overall switch count from twelve to nine. In addition, the dual functionality feature significantly enhances the system robustness against severe symmetrical/asymmetrical grid faults and voltage dips. A detailed study on all the possible operational modes of six-port converter is presented. An appropriate control algorithm is developed and the validity of the proposed configuration is verified through extensive simulation as well as experimental studies under different operating conditions.**

***Index Terms*—Bidirectional power flow, distributed power generation, photovoltaic (PV) systems, power quality, voltage control.**

I. Introduction

THE FAST depletion of conventional energy resources and increasing environmental concerns have made renewable energy resources, such as photovoltaic (PV) and wind, progressive sources of electric power generation [1]–[4]. Since power generated by a PV source is principally dc, it requires a dc–ac inversion stage for grid-connected operation. The main component of a grid-connected PV system is generally the three phase voltage source inverter (VSI) having six switches in total. Its primary function is to enhance the injected active power through maximum power point tracking (MPPT) control of PV array [5]. On the other hand, with the increased penetration of sensitive loads, the power quality issues in the modern distribution system have significantly increased [6]. Most frequent and serious disturbances in the grid voltage are sags, swells, and faults. To maintain uninterrupted voltage at load terminals, various custom power devices are used among which DVR is considered as the most effective and comprehensive solution [7]–[11].

It is likely that the modern load centers would be equipped with on-site PV generation unit(s) as well as custom power device(s) for critical load protection. Fig. 1 shows such a system configuration where a grid-connected PV plant injects active power through six-switch VSI (PV-VSI) while self-supported DVR performs voltage sag compensation for sensitive loads using second six-switch VSI (DVR-VSI). During the occurrence of fault/deep sag at the point of common coupling (PCC), these independent PV and DVR systems face major operational limitations. In this scenario, the self-supported DVR can no longer maintain the rated load voltage due to finite energy in dc-link capacitor. Similarly, the active power produced by PV plant cannot be supplied to the grid. One possible solution for DVR is to keep the dc-link capacitor charged at rated value through a shunt rectifier connected at load side [12]. However, this configuration faces large VA loading of DVR-VSI, which must be rated for both load and shunt rectifier VA. Another way to enhance the DVR performance is to replace the dc-link capacitor with a battery energy storage system [13]. Although, it does not affect DVR rating but incurs additional battery maintenance issues.

The VA rating of centralized PV inverter depends on the installed capacity of PV solar panels. This inverter VA is generally underutilized due to intermittent nature of solar power especially during late evening hours, night hours, and early morning hours where it remains idle. On the other hand, the DVR VA rating is typically 20%–40% of the total load VA loading. The DVR inverter also has low-utilization factor as the voltage disturbance is a short duration power quality issue and does not occur frequently.

By combining the above two applications, in this paper, a new six-port converter-based system configuration is proposed for integrating on-site PV generation unit and DVR as shown in Fig. 2. The proposed configuration eliminates the requirement of two separate inverters for PV and DVR applications, reduce the switch count of conventional system by 25% and most importantly overcomes the above-mentioned operational limitations associated with conventional PV and DVR systems. The proposed configuration could be useful for low to medium power load centers/factories with sensitive loads and considerable onsite PV generation capacity (more than 50% of the load requirement). Under this consideration, the VA rating of PV system will govern the overall VA rating of six-port converter, which means that equally rated (as of PV system) DVR is available for load voltage regulation.

In the literature, the six-port converter is reported as a replacement of traditional back to back converters for dual motor drives [14], rectifier–inverter systems [15], uninterruptible power supplies [16], [17], UPQC [18], and for microgrid applications [19]. Fault ride through enhancement of DFIG-based wind energy conversion system using nine switch-based converter is also reported recently in [20]. Nevertheless, the proposed configuration of Fig. 2 retains all the essential features of traditional 12 switch system in Fig. 1. It replaces the two

Manuscript received July 21, 2014; revised November 15, 2014; accepted November 22, 2014. Date of publication January 22, 2015; date of current version March 18, 2015. Paper no. TSTE-00364-2014.

The authors are with the Institute Center for Energy, Masdar Institute of Science and Technology, Abu Dhabi, United Arab Emirates (e-mail: arauf@masdar.ac.ae; vkhadkikar@masdar.ac.ae).

Color versions of one or more of the figures in this paper are available online at http://ieeexplore.ieee.org.

Digital Object Identifier 10.1109/TSTE.2014.2381291

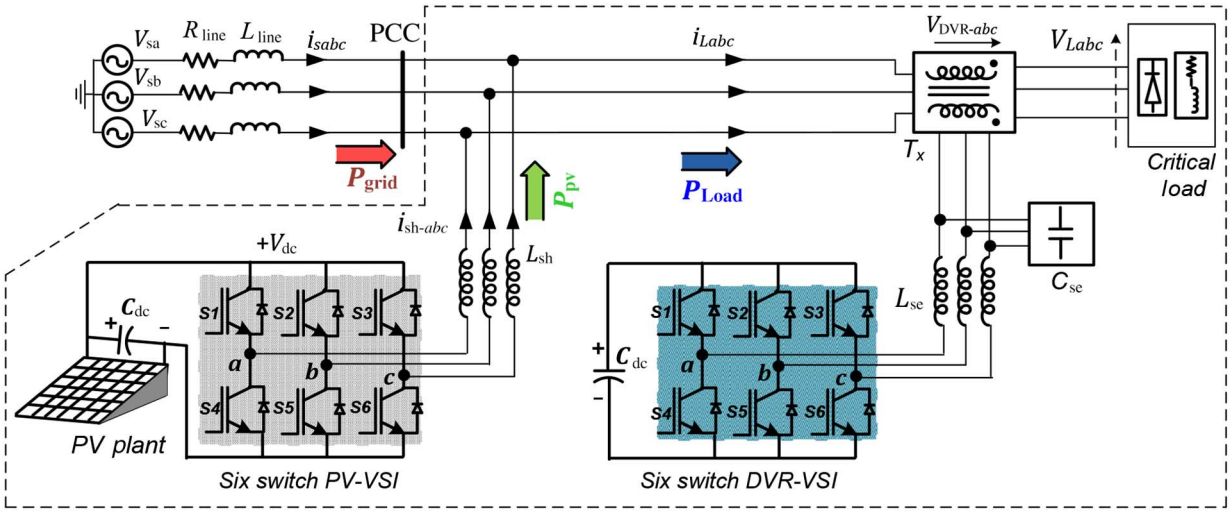

Fig. 1. On-site PV generation and sensitive load protection using self-supported DVR system.

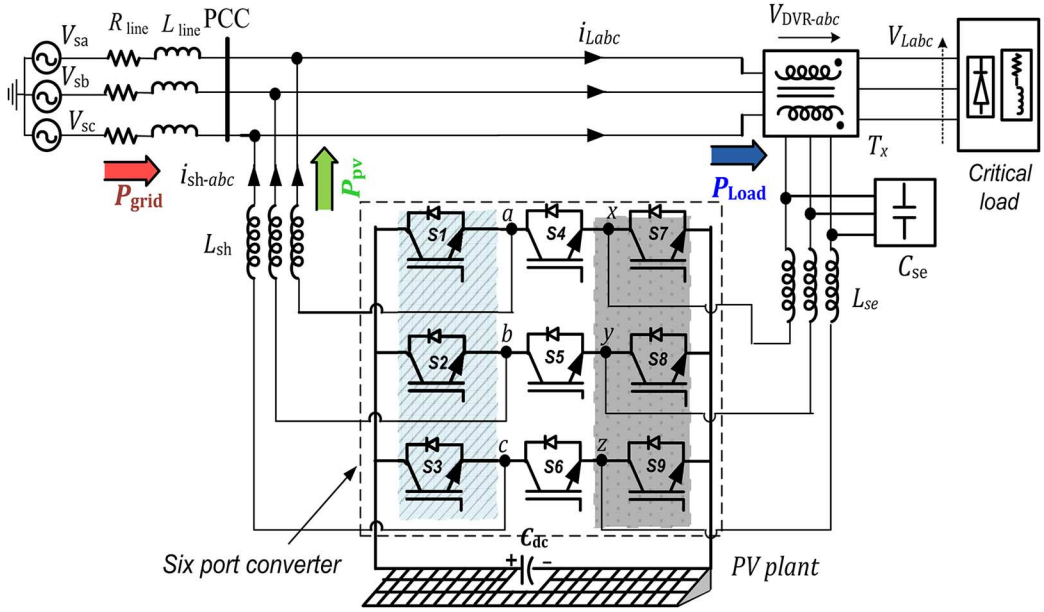

Fig. 2. Proposed integrated PV and DVR system configuration.

dissimilar VSIs with one integrated converter while reducing the overall semiconductor count, gate drive, and control circuitry (by 25%). Furthermore, the configuration allows bidirectional active power flow between six-port converter, PV plant, and utility grid, a feature that provides seamless sag compensation to protect sensitive loads during severe voltage dips at PCC. The proposed work is evaluated by detailed simulation study and finally, validated experimentally.

II. Proposed Integrated PV-DVR System Configuration

The proposed system configuration is shown in Fig. 2. In this configuration, nine semiconductor switches are used to realize PV and DVR operations simultaneously. The main difference between the proposed configuration and the system given in Fig. 1 is the dual output six-port converter whose six out-ports are divided into two set of outputs. The left three ports $\{a, b, c\}$ connected to PCC are designated as the output of PV-VSI, whereas the right three ports $\{x, y, z\}$ are designated as output of DVR-VSI. Switches $S_4 - S_6$ are shared between PV and DVR VSIs. Based on the grid condition and PV plant status, the six-port converter can operate in one of the various operational modes as given in Table I.

A. Mode-1 (Healthy Grid Mode)

Mode-1 reflects the normal operation of six-port converter when the grid voltage is at nominal value and PV plant is operating at standard atmospheric condition (SAC). During *Mode-1*, PV-VSI injects the active power generated by PV plant in the grid while DVR-VSI remains inactive as the grid is healthy. Fig. 3 shows the equivalent operational circuit of six-port converter depicting the status of each switch.

TABLE I
PROPOSED INTEGRATED PV-DVR SYSTEM CONFIGURATION: DIFFERENT MODES OF OPERATION

Mode	PV status	Grid condition	Switch status		Six-port converter operation	
			Always "ON"	PWM	PV-VSI	DVR-VSI
1	Active	Healthy $V_{\text{pcc-p.u.}} = 1$	S_7–S_9	S_1–S_6	Active ($P_{\text{PV-VSI}} > 0$)	Idle ($\text{PQ}_{\text{DVR-VSI}} = 0$)
2	Active	Fault $V_{\text{pcc-p.u.}} \approx 0$	S_1–S_3	S_4–S_9	Idle ($P_{\text{PV-VSI}} = 0$)	Active ($\text{PQ}_{\text{DVR-VSI}} = \text{PQ}_{\text{LOAD}}$)
3	Active	Sag $0.1 < V_{\text{pcc-p.u.}} < 0.95$	None	S_1–S_9	Active ($P_{\text{PV-VSI}} > 0$)	Active ($\text{PQ}_{\text{DVR-VSI}} < \text{PQ}_{\text{LOAD}}$)
4	Inactive	Any of the above 3	None	S_1–S_9	Active ($P_{\text{PV-VSI}} < 0$)	Active

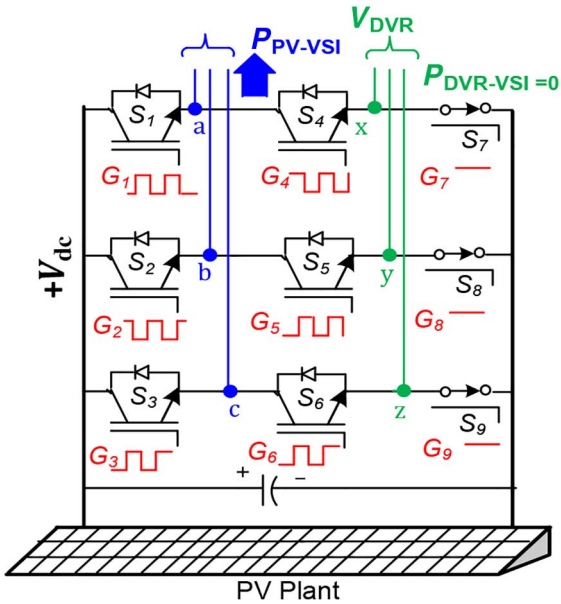

Fig. 3. *Mode-1*: Equivalent system representation.

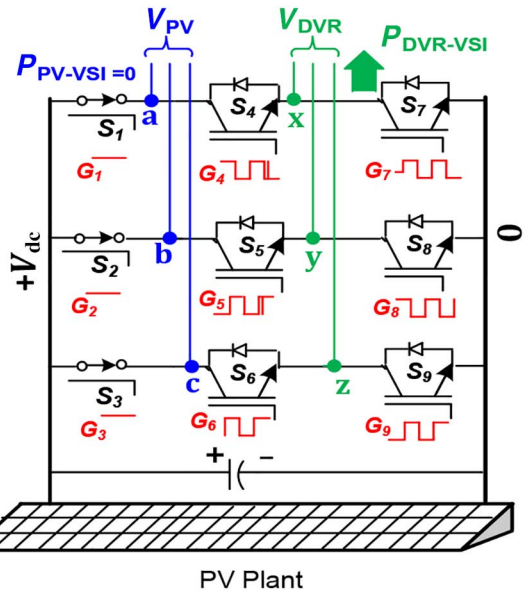

Fig. 4. *Mode-2*: Equivalent system representation.

The carrier-based modulation scheme (further explained in Section III) generates the necessary gating signal pattern for all the switches. As shown in Fig. 3 and Table I, switches S_7–S_9 are "ON (logical high)" throughout *Mode-1* while remaining six switches (S_1–S_6) are operated in pulse width modulation (PWM) control to perform PV-VSI operation. The ON status of S_7–S_9 effectively short circuits the primary windings of series injection transformer and thus, the active power supplied by DVR-VSI ($P_{\text{dvr-vsi}}$) is zero.

B. Mode-2 (Fault Mode)

Mode-2 corresponds to a condition when there is a three-phase fault at PCC. During this mode, PV-VSI remains inactive while DVR-VSI injects the maximum compensating voltages (V^*_{Labc}). The gating signals for three left-most switches of six-port converter remain at logic high. Therefore, switches S_1–S_3 are "ON" throughout the *Mode-2* as shown in Fig. 4. Since the PV plant is operating at SAC, the six-port converter feeds the critical load independently (with no support from utility grid) through the switches S_4–S_9 and functions as PV supported DVR. Since the conventional PV and self-supported DVR system cannot perform during three-phase fault at PCC, *Mode-2* is unique feature of the proposed configuration that cannot be realized in Fig. 1. Under such condition, the necessary neutral point for series transformer is provided through PV-VSI coupling inductor with S_1–S_3 remain ON throughout. Note that there would be a small voltage drop across these inductors, which can be easily compensated by DVR itself.

C. Mode-3 (Sag Mode)

Mode-3 considers the operation of six-port converter during a voltage sag at PCC. In this mode, the DVR-VSI performs the presag compensation to avoid premature tripping of critical load due to large phase jump. Since the grid voltage is nonzero, the PV plant contributes to inject limited active power based on the maximum current capacity, i.e., both DVR and PV-VSI (all nine switches) are active during *Mode-3* as shown in Fig. 5.

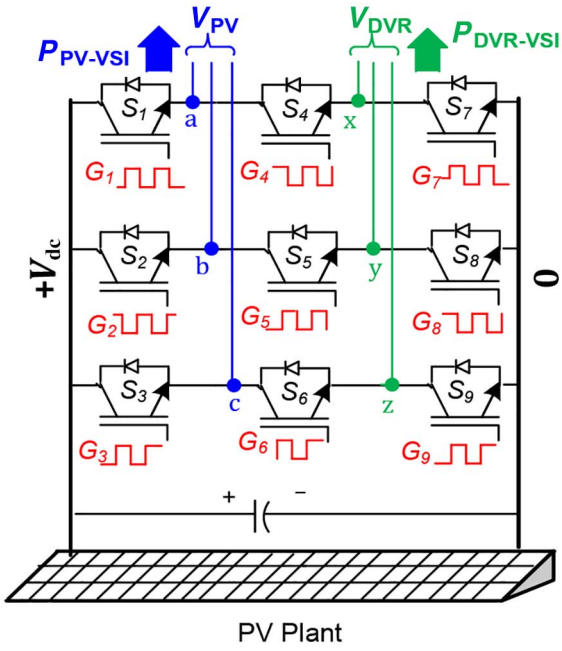

Fig. 5. *Mode-3*: Equivalent system representation.

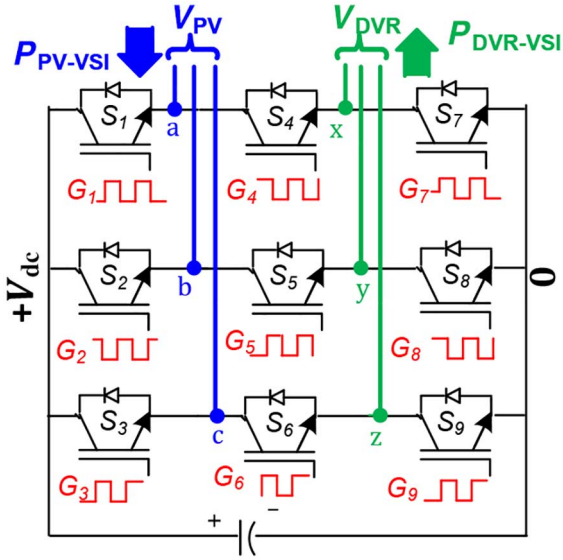

Fig. 6. *Mode-4*: Equivalent system representation.

Based on the magnitude of sag depth and load power factor, the active power from PV plant is shared between load and grid, where the sensitive load is given the first priority (explained in Section IV).

D. Mode-4 (No PV Generation)

Mode-4 corresponds to the operation of six-port converter when PV plant does not provide any active power and remains inactive (during early morning hours, late evening hours, fully cloudy day, and throughout night hours). In the absence of PV plant, the role of PV-VSI is reversed. It remains idle as long as the grid is operating at rated voltage and draws active power from grid during sag intervals to keep the dc-link capacitor charged at rated value. The equivalent representation of this mode is similar to *Mode-3* as shown in Fig. 6 with the modification that PV-VSI active power flow is reversed (from grid towards dc link).

In the case of severe or deeper sag depths where the current requirement exceeds the switch current rating, the dc-link regulation cannot be performed. The capacitor size $C_{\rm dc}$ in such cases is calculated based on the following equation:

$$C_{\rm dc} = \frac{t_{c\text{-max}} * 2 * P_{\text{dvr-vsi}}}{\left[V_{\rm dc}^2 - \left(\frac{2 * V_{\text{dvr-vsi}}}{m_{i\text{-max}} * n_t}\right)^2\right]} \tag{1}$$

where $t_{c\text{-max}}$ is the maximum compensation time. $m_{i\text{-}max}$ is the maximum modulation index of DVR-VSI. n_t is the transformer turns ratio and $P_{\text{dvr-vsi}}$ is the active power required to maintain the nominal load voltage. Further details on the capacitor sizing are given in [10].

III. Operating Principle and Modulation Scheme for Six-Port Converter

As shown in Fig. 2, the six-port converter has three switches shared between PV and DVR-VSIs. It, therefore, faces restriction on the allowable switching states. The two output ports on the same leg can have four possible connections. 1) Both outputs connected to $+V_{\rm dc}$ (for phase-a: S_1-ON, S_4-ON, and S_7-OFF); 2) both to 0 V (for phase-a: S_1-OFF, S_4-ON, and S_7-ON); 3) left port to $+V_{\rm dc}$ and right port to 0 V (for phase-a: S_1-ON, S_4-OFF, and S_7-ON); and 4) left port to 0 V and right port to $+V_{\rm dc}$ (for phase-a: S_1-ON, S_4-ON, and S_7-ON). The last combination, however, cannot be realized as it will result in direct short-circuiting of dc link. To achieve modulation, both the reference signals are compared with a common carrier for generating the gate pulses. In the common carrier band, the modulation reference signal of left port is placed above that of right using third harmonic injection method [16] with no impact on output (line voltages) of six-port converter. To prevent the dc-link short circuit (due to combination 4), the crossover between two modulating reference signals should be avoided.

Two types of operations of six-port converter are possible to overcome the aforementioned limitation. 1) Equal frequency (EF) operation, where both set of outputs (i.e., $V_{\text{pv-}abc}$ and $V_{\text{dvr-xyz}}$) must operate at same frequency with small inter phase difference as shown in Fig. 7(a). 2) Variable frequency (VF) operation of both set of outputs. This operation is more flexible as there is no constraint on the output frequency and could be useful for harmonic compensation [Fig. 7(b)]. However, the sum of modulation references for left and right port must not exceed unity [18]. VF operation requires doubling of dc-link voltage to prevent reference crossover as shown in Fig. 7(b). Further details on these operations (EF and VF) and six-port configuration can be found in [16]–[18].

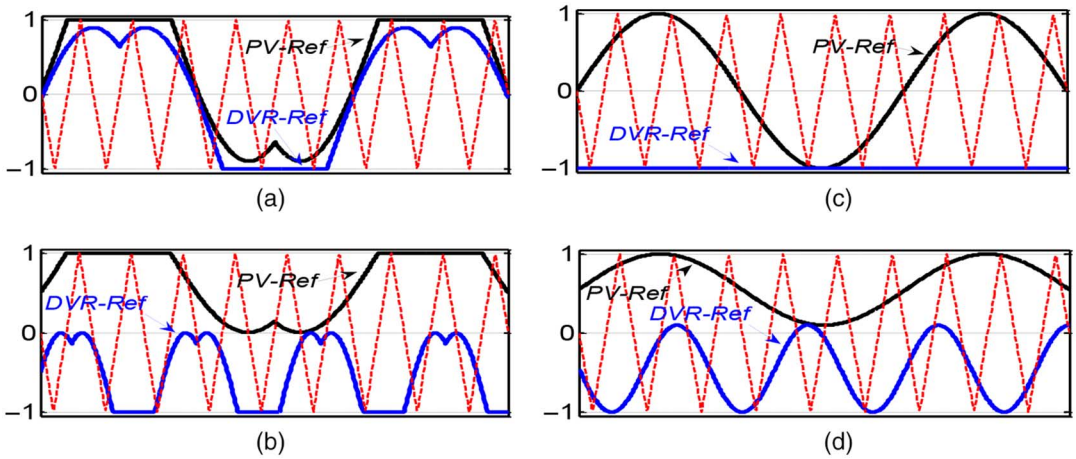

Fig. 7. Per phase representation of PV and DVR-VSI modulation references during (a) EF operation; (b) VF operation; (c) healthy grid mode; and (d) sag mode.

During the normal mode, PV-VSI injects active power into grid while DVR-VSI is idle (*Mode-1*). The modulation index is unity for PV-VSI and zero for DVR-VSI as shown in Fig. 7(c). During sag (*Mode-3*) the PV-VSI continues to inject active power similar to *Mode-1*, but at a reduced modulation index, as the PCC voltage is reduced due to voltage sag. This facilitates the DVR-VSI to attain higher modulation index (required to compensate the sag) as shown in Fig. 7(d). The increase in DVR-VSI reference is always accompanied by the corresponding decrease in PV-VSI reference and hence the crossover does not happen.

Thus, the proposed configuration naturally overcomes the limitation of reference crossover. To achieve the above operation in the proposed configuration, the procedure to generate nine gate pluses is discussed below. The two reference signals can be expressed as

$$\left.\begin{aligned} V^*_{\text{pv-a}} &= m_{\text{pv}} \cos\left(w_{\text{pv}} t + \varnothing_{\text{pv}}\right) \\ V^*_{\text{pv-b}} &= m_{\text{pv}} \cos\left(w_{\text{pv}} t - 120^\circ + \varnothing_{\text{pv}}\right) \\ V^*_{\text{pv-c}} &= m_{\text{pv}} \cos\left(w_{\text{pv}} t - 240^\circ + \varnothing_{\text{pv}}\right) \end{aligned}\right\} \tag{2}$$

$$\left.\begin{aligned} V^*_{\text{dvr-x}} &= m_{\text{dvr}} \cos\left(w_{\text{dvr}} t + \varnothing_{\text{dvr}}\right) \\ V^*_{\text{dvr-y}} &= m_{\text{dvr}} \cos\left(w_{\text{dvr}} t - 120^\circ + \varnothing_{\text{dvr}}\right) \\ V^*_{\text{dvr-z}} &= m_{\text{dvr}} \cos\left(w_{\text{dvr}} t - 240^\circ + \varnothing_{\text{dvr}}\right) \end{aligned}\right\} \tag{3}$$

where $V^*_{\text{pv}a,b,c}$ and $V^*_{\text{dvr}\,x,y,z}$ are PV-VSI and DVR-VSI reference signals determined by the respective control blocks (explained later in Section IV). m_{pv}, w_{pv}, and $\varnothing_{\text{pv}}$ are the modulation ratio, angular frequency, and phase angle of the PV-VSI, whereas m_{dvr}, w_{dvr}, and $\varnothing_{\text{dvr}}$ are the corresponding values for DVR-VSI, respectively. The modified offset references can be determined from (2) and (3), as

$$\left.\begin{aligned} V_n &= 1 - \left[\text{Max}\left(V^*_{\text{pv}a,b,c}\right)\right] \\ M_{\text{pv-}a,b,c} &= V_n + V^*_{\text{pv}a,b,c} \end{aligned}\right\} \tag{4}$$

$$\left.\begin{aligned} V_m &= -1 - \left[\text{Min}\left(V^*_{\text{dvr}x,y,z}\right)\right] \\ M_{\text{dvr-}x,y,z} &= V_n + V^*_{\text{dvr}x,y,z} \end{aligned}\right\} \tag{5}$$

where $M_{\text{pv-}a,b,c}$ and $M_{\text{dvr-}x,y,z}$ are the offset 120° discontinues reference signals fed to individual PWM comparators PWM_{pv} and PWM_{dvr} giving two sets of six gating signals, respectively

$$G_{\text{pv}1-3} = !(G_{\text{pv}4-6})' = \begin{cases} 1, & \text{if} \quad M_{\text{pv-a,b,c}} > M_c \\ 0, & \text{if} \quad M_{\text{dvr-}a,b,c} < M_c \end{cases} \tag{6}$$

$$G_{\text{dvr}1-3} = !(G_{\text{dvr}4-6})' = \begin{cases} 1, & \text{if} \quad M_{\text{dvr-}x,y,z} > M_c \\ 0, & \text{if} \quad M_{\text{dvr-}x,y,z} < M_c \end{cases} \tag{7}$$

where M_c is the carrier signal amplitude. These twelve gating signals can be directly sent to corresponding inverters if PV and DVR VSIs are operated using two separate six switch inverters like in Fig. 1. However, in the six-port converter, since the middle row switches are shared, their gate pulses are generated by logical OR operation of PWM signals corresponding to right three switches of PV-VSI, i.e., $G_{\text{pv}4-6}$ and left three switches of DVR-VSI, i.e., $G_{\text{dvr}1-3}$. The final nine gating signals G_{n1-9} are obtained as follows:

$$\left.\begin{aligned} G_{n1-3} &= G_{\text{pv}1-3} \\ G_{n7-9} &= G_{\text{dvr}4-6} \\ G_{n4,5,6} &= G_{\text{pv}4-6} + G_{\text{dvr}1-3} \end{aligned}\right\}. \tag{8}$$

IV. Overall Control System

A. Control of PV-VSI

The PV-VSI active and reactive power in synchronous reference frame is given as

$$\left.\begin{aligned} P &= 1.5 * [v_d i_d + v_q i_q] \\ Q &= 1.5 * [v_d i_q - v_q i_d] \end{aligned}\right\}. \tag{9}$$

Using the voltage oriented control [5], the reference frame d-axis is aligned with positive sequence PCC voltage, i.e., $V_d = V_{\text{pcc}}$. Therefore, $i^*_{d\text{-pv}}$ which gives a direct measure of PV power can be expressed as

$$i^*_{d\text{-pv}} = \frac{2}{3 * V_d} P_{\text{pv}}. \tag{10}$$

This reference current $i^*_{d\text{-pv}}$ is obtained through MPPT voltage control loop. The details about MPPT control are explained

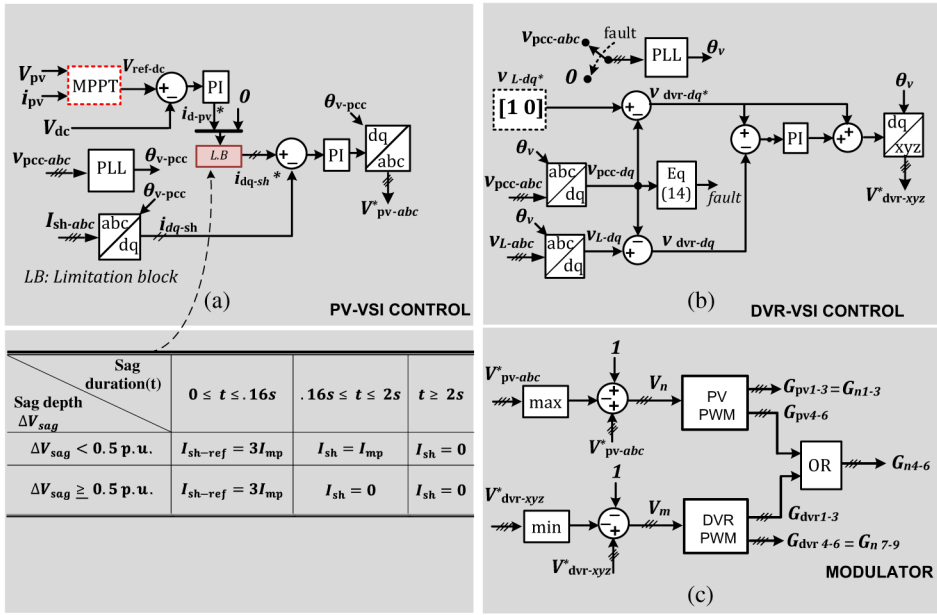

Sag depth ΔV_{sag} \ Sag duration(t)	$0 \le t \le .16s$	$.16s \le t \le 2s$	$t \ge 2s$
$\Delta V_{sag} < 0.5$ p.u.	$I_{sh-ref} = 3I_{mp}$	$I_{sh} = I_{mp}$	$I_{sh} = 0$
$\Delta V_{sag} \ge 0.5$ p.u.	$I_{sh-ref} = 3I_{mp}$	$I_{sh} = 0$	$I_{sh} = 0$

Fig. 8. Control block representation. (a) PV-VSI; (b) DVR-VSI; and (c) six-port converter modulator.

in [5]. The q-axis reference current i_q^* is set to zero as per IEEE 1547 [21]. Further, as per the interconnection requirements (e.g., IEEE 1547), the PV injected current should be regulated based on sag depths and duration. Different limits on the shunt PV current are regulated by the limitation block (LB), as shown in Fig. 8(a). The six-port converter's semiconductor devices can be overloaded up to three times their rated current capacity ($I_{\rm mp}$) based on the thermal rating of the switches. The actual injected current is measured and transformed to synchronous frame $\{i_{\text{sh-}d}, i_{\text{sh-}q}\}$. Both actual and reference values are compared and error is processed through a PI controller. The resulting output signals is transformed back to stationary reference frame giving $V^*_{\text{pv}a,b,c}$ as shown in Fig. 8(a).

B. Control of DVR-VSI

The control block for DVR-VSI is shown in Fig. 8(b). The difference between reference ($V^*_{\text{dvr-}dq} = V^*_{L\text{-}dq} - V_{\text{pcc-}dq}$) and actual DVR voltage ($V_{\text{dvr-}dq} = V_{L\text{-}dq} - V_{\text{pcc-}dq}$) is processed by PI controller in the synchronous reference frame. $V^*_{\text{dvr-}dq}$ can be directly used to control DVR-VSI in open loop by converting it in to stationary reference frame. However, it will not be able to compensate the drop across DVR-VSI switches, interfacing filter and series transformer. It is, therefore, added as feed forward signal to the output of PI to compensate for system losses. The resulting signal is converted into stationary frame giving $V^*_{\text{dvr}a,b,c}$.

For sag/fault detection the absolute error between reference PCC voltage (1 p.u.) and actual PCC voltage magnitude (p.u.) in synchronous reference frame is calculated as follows:

$$V_{\text{error}} = \left|1 - \sqrt{V^2_{\text{pcc-}d} - V^2_{\text{pcc-}q}}\right|. \tag{11}$$

As soon V_{error} exceeds the threshold of 0.05, p.u. sag is detected and the *fault* signal in Fig. 8 changes its logic from 0 to 1. Once $V^*_{\text{pv-}abc}$ and $V^*_{\text{dvr-}xyz}$ reference modulating signals for PV and DVR VSIs are obtained, they are processed by modulator to generate nine gate signals, as shown in Fig. 8(c).

TABLE II
SYSTEM PARAMETERS USED FOR SIMULATION STUDY

Parameter	Value
Grid voltage (L–L) (rms) V_{base}	415 V
Line frequency	50 Hz
Nominal PV power (Base kVA)	10 kVA
Nominal load power	10 kVA
Nominal load power factor	0.8 lagging
DC link voltage	700 V
DC link capacitance	3000 μF
Maximum shunt current, ($I_{\text{sh–max}}$)	20 A
Series transformer rating/turn ratio	10 kVA/ 1:1
Filter inductor L_f and capacitance C_f	5 mH and 50 μF
Grid impedance Z_{line}	$0.5 + j0.05\ \Omega$

V. SIMULATION STUDY

In this section, MATLAB/Simulink-based study is presented to illustrate the feasibility of proposed system configuration. The parameters of simulated system are given in Table II.

A. Mode-1 (Healthy Grid Mode)

During *Mode-1*, the grid is operating at normal condition (PCC voltage = 1 p.u.). Fig. 9(a)–(e) shows the simulation results for *Mode-1*. All the results are expressed in p.u. with the base value of 10 kVA and 415 V. The PV plant operates in the range of 60%–100% of SAC. The reference value of d-axis

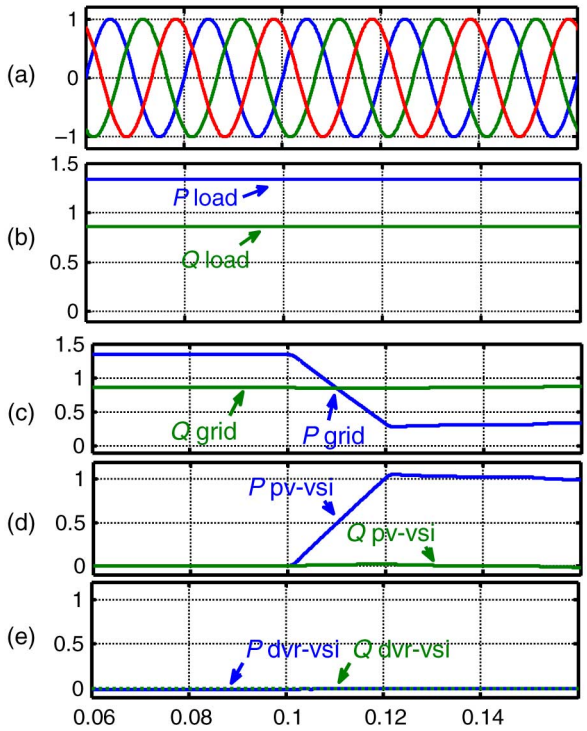

Fig. 9. Simulation results: operation of proposed system during health grid mode (PV-VSI: active and DVR-VSI: inactive). (a) $V_{\rm pcc}$; (b) $PQ_{\rm load}$; (c) $PQ_{\rm grid}$; (d) $PQ_{\rm pv\text{-}VSI}$; and (e) $PQ_{\rm dvr\text{-}VSI}$.

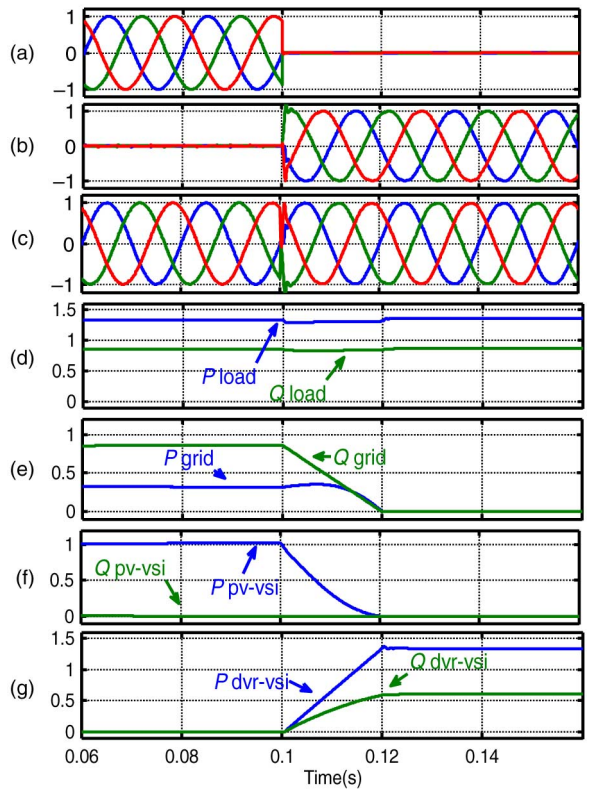

Fig. 10. Simulation results: operation of proposed system during fault mode (PV-VSI: inactive and DVR-VSI: active). (a) $V_{\rm pcc}$; (b) $V_{\rm dvr}$; (c) $V_{\rm load}$; (d) $PQ_{\rm load}$; (e) $PQ_{\rm grid}$; (f) $PQ_{\rm pv\text{-}VSI}$; and (g) $PQ_{\rm dvr\text{-}VSI}$.

current $i^*_{d\text{-pv}}$ set by MPPT loop is 20 A. At $t = 0.1$ s, PV-VSI is turned ON. It starts injecting PV active power (1 p.u.) into grid as shown in Fig. 9(d). The grid active power is reduced by the same amount as shown in Fig. 9(b). Note that the DVR-VSI remains inactive during this mode.

B. Mode-2 (Fault Mode)

In this mode, PV plant supports the critical load independently and six-port converter performs the operation of DVR by supplying the full load active and reactive power. As can be seen from Fig. 10(e)–(g), once the fault occurs at $t = 0.1$ s, the PV-VSI becomes inactive and the power generated by PV plant is completely handled by DVR-VSI. This mode is unique to the proposed configuration as it increases the PV plant efficiency by optimally utilizing its power for feeding critical load which otherwise cannot delivered to grid. Although not considered in this paper, PV-VSI can perform the STATCOM operation, by injecting reactive power in the grid and may take part in fault ride through enhancement.

C. Mode-3 (Sag Mode)

1) Balanced Three Phase Voltage Sag: Assume that there is symmetrical sag depth of 50% in the grid voltage, i.e., PCC voltage decreases to 0.5 p.u. The sag occurs at $t = 0.1$ s and *Mode*-3 begins as soon as the sag is detected. Fig. 11(a)–(e) shows the simulation results for *Mode-3*. The proposed configuration restores the presag load voltage by injecting the required fundamental voltage through series transformer. Both DVR-VSI and PV-VSI take part in the sag compensation. It can be seen that PV-VSI continues to inject the PV plant active power into grid during this mode. Although the sag depth is 50%, due to presag restoration, 80% of PV plant active power is delivered to the load through DVR-VSI as shown in Fig. 11(f). The remaining 20% PV power goes into grid through PV-VSI as shown in Fig. 11(e).

2) Unbalanced Three Phase Voltage Sag: The operation of six-port converter during unbalanced sag with the positive sequence voltage drop of 40% and negative sequence voltage injection of 30% is depicted in Fig. 12(a)–(f). The sag occurs at $t = 0.1$ s and DVR-VSI performs the presag compensation similar to the case of symmetrical sag depth. It should be noted that the proposed configuration operates in *Mode-3* only (as long as $0.1 < V_{\rm pcc-p.u.} < 0.95$). In case $V_{\rm pcc-p.u.} < 0.1$, the controller takes this as a fault and makes a transition from *Mode-3* to *Mode-2*.

D. Mode-4 (No PV Generation)

This mode corresponds to the intervals when PV plant is not producing any active power. As explained earlier, during this mode, PV-VSI takes the role of dc-link voltage regulation by drawing power from grid. Fig. 13(a)–(f) shows the simulation results for *Mode-4*. Before the sag DVR-VSI is inactive and PV-VSI operates through remaining six switches. It draws a small amount of power from the grid to overcome the system losses and maintain the dc link. As soon as the sag is detected at $t = 0.3$ s, the six-port converter performs the load voltage

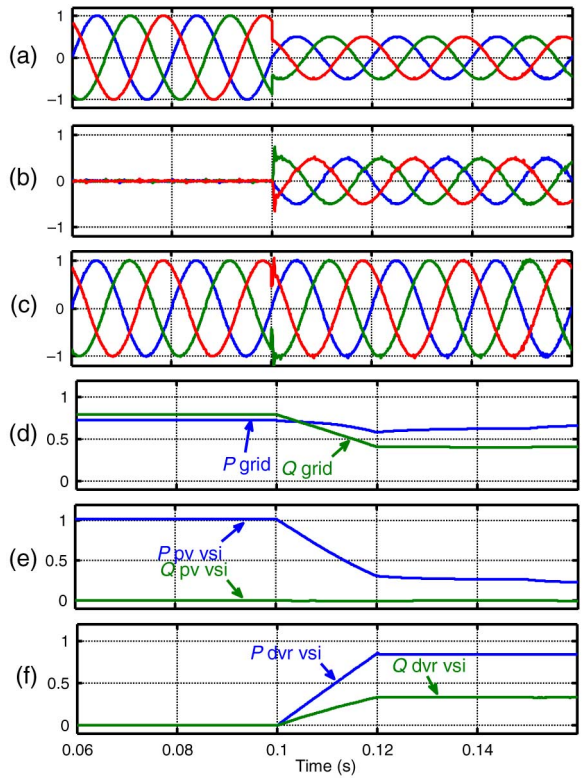

Fig. 11. Simulation results: operation of proposed system during balance three phase sag mode (PV-VSI: active and DVR-VSI: active). (a) $V_{\rm pcc}$; (b) $V_{\text{dvr-VSI}}$; (c) $V_{\rm load}$; (d) $PQ_{\rm grid}$; (e) $PQ_{\text{pv-VSI}}$; and (f) $PQ_{\text{dvr-VSI}}$.

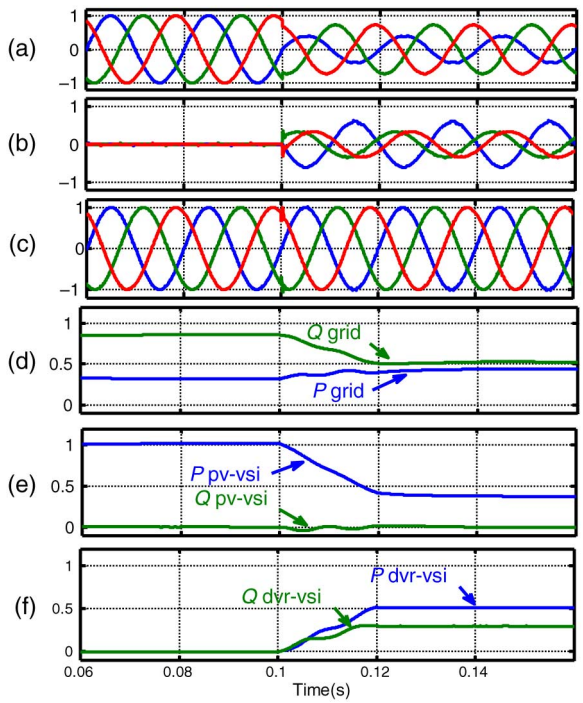

Fig. 12. Simulation results: operation of proposed system during unbalanced sag mode (PV-VSI: active and DVR-VSI: active). (a) $V_{\rm pcc}$; (b) $V_{\text{dvr-vsi}}$; (c) $V_{\rm load}$; (d) $PQ_{\rm grid}$; (e) $PQ_{\text{pv-VSI}}$; and (f) $PQ_{\text{dvr-VSI}}$.

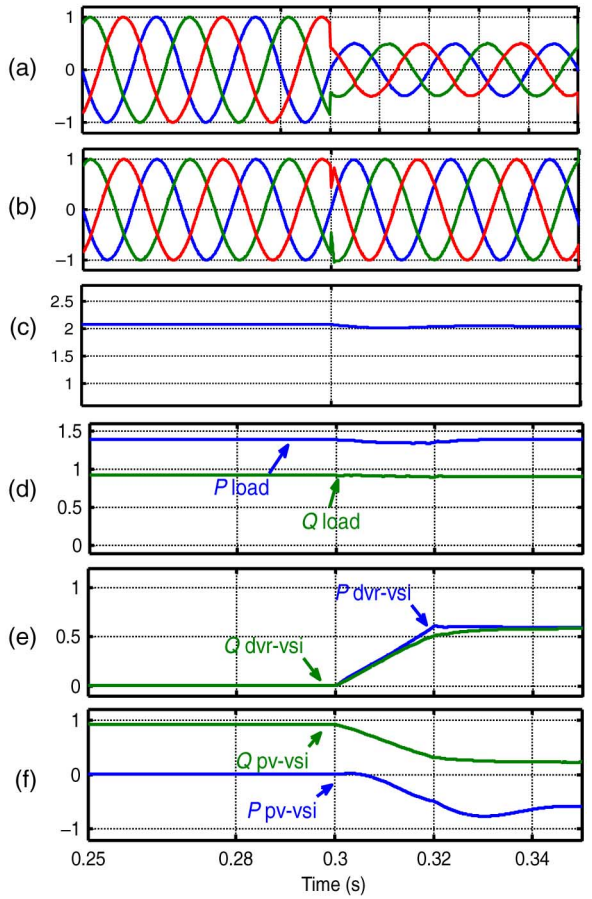

Fig. 13. Simulation results: operation of proposed system during inactive PV plant mode (PV-VSI: active and DVR-VSI: active). (a) $V_{\rm pcc}$; (b) $V_{\rm load}$; (c) $V_{\rm dc}$; (d) $PQ_{\rm load}$; (e) $PQ_{\text{dvr-VSI}}$; and (f) $PQ_{\text{pv-VSI}}$.

compensation by injecting the necessary voltage through DVR-VSI as shown in Fig. 13(e). The PV-VSI maintains the dc-link voltage as shown in Fig. 13(c). The required load active power during this mode is actually supplied from the grid through PV-VSI and DVR-VSI combination.

VI. Experimental Validation

To validate the performance of proposed configuration, a scaled experimental prototype is developed in the laboratory using digital signal processor (DSP) DS1103 dSPACE and Semikron SKM75 switch-based six-port-converter. A 16-Channel *Yokogawa DL850* oscilloscope is used to capture the experimental results. Since the controller card of DS1103 supports a maximum of six PWM signals compared to nine required for six-port-converter, an external gate drive circuitry with the dead band of 2 μs is also developed in the laboratory. The final hardware setup is shown in Fig. 14 and the experimental system parameters are listed in Table III. A sampling time of 50 μs is used in the DSP to implement the algorithm in real-time. A three-phase programmable voltage source is used to emulate the grid for flexible testing purpose. The experimental

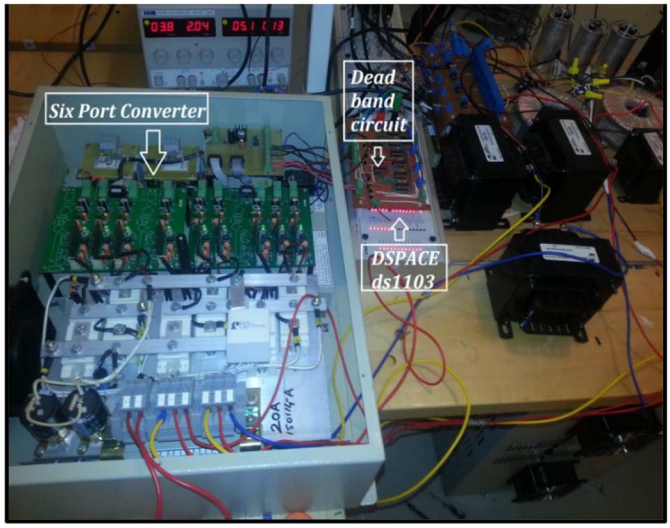

Fig. 14. Experimental setup of proposed system configuration.

TABLE III
SYSTEM DATA FOR EXPERIMENTAL STUDY

Source Chroma 61703	Supply voltage: 40 V-pn, 50 Hz Source impedance: $R_g = 0.047\ \Omega$ and $L_g = 160\ \mu H$
Six-port-converter	dc link capacitors, $C_{dc} = 1100\ \mu F$ Reference dc link voltage = 80-100 V Series filter inductor, $L_s = 5$ mH and $C_s = 50\ \mu F$ Shunt filter inductor, $L_f = 5$ mH and $C_f = 15\ \mu F$ Transformer turns ratio 1:1
Load	$R = 27\ \Omega$

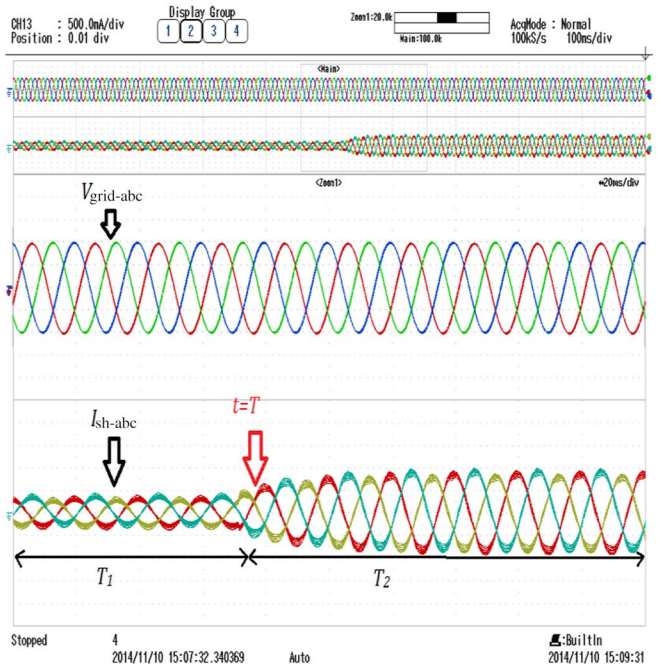

Fig. 15. Experimental results: operation of proposed six-port converter during steady state conditions.

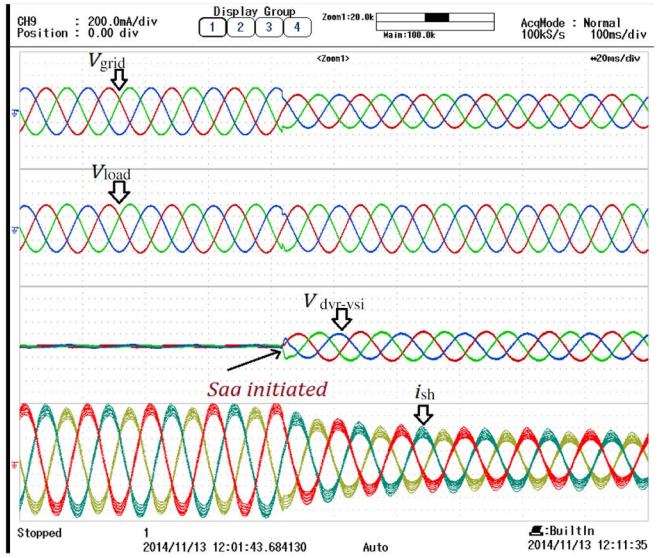

Fig. 16. Experimental results for operation of proposed six-port converter during symmetrical sag in the grid voltage.

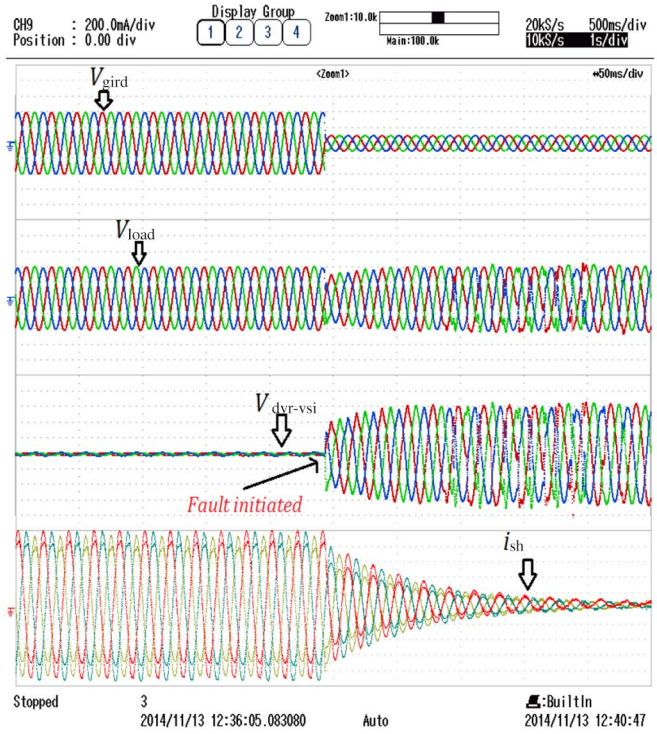

Fig. 17. Experimental results for operation of proposed six-port converter during fault in the grid voltage.

results for steady state conditions ($V_{pcc} = 1$ p.u.) are shown in Fig. 15. A step in the injected active power is initiated at $t = T$ from $P_1 = 50$ W to $P_2 = 150$ W. It can be seen that six-port converter effectively increases the injected current through PV-VSI.

Fig. 16 shows the experimental results for symmetrical sag in the grid voltage. The proposed six-port converter effectively mitigates the sag by injecting the missing voltage through

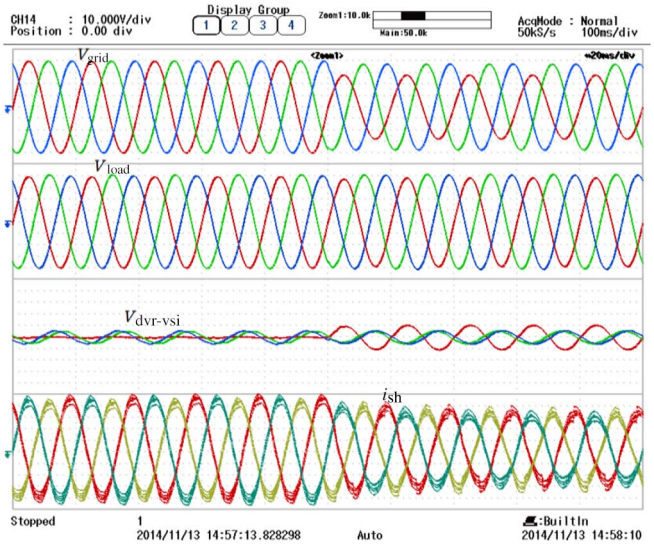

Fig. 18. Experimental results for operation of proposed six-port converter during unsymmetrical sag in the grid voltage.

the DVR-VSI. As discussed earlier, all the nine switches of six-port converter remain active during this mode. There is a reduction in active power injected by PV-VSI as shown in Fig. 16(c) since DVR-VSI consumes the PV power for sag compensation. The performance of the proposed configuration during deep sag/fault in the grid voltage is shown in Fig. 17. As soon as the fault occurs at $t = T$, the active power injected by PV-VSI drops down to zero as shown in Fig. 17(c). The DVR-VSI instead inject this active power to maintain the rated voltage at the load terminals. Finally, the experimental result for the unbalanced sag in the grid voltage is depicted in Fig. 18. At $t = T$, the grid voltage is programmed with a positive sequence drop of 20% and negative sequence voltage injection of 15%. The unbalance in the grid voltage can be noticed from Fig. 18. The proposed six-port converter maintains the load voltage remains at the rated value. Thus, the above-experimental study demonstrates the effectiveness of the proposed configuration for practical applications.

VII. Conclusion

In this paper, a new system configuration for integrating a conventional grid-connected PV system and self supported DVR is proposed. The proposed configuration not only exhibits all the functionalities of existing PV and DVR system, but also enhances the DVR operating range. It allows DVR to utilize active power of PV plant and thus improves the system robustness against sever grid faults. The proposed configuration can operate in different modes based on the grid condition and PV power generation. The discussed modes are healthy grid mode, fault mode, sag mode, and PV inactive mode. The comprehensive simulation study and experimental validation demonstrate the effectiveness of the proposed configuration and its practical feasibility to perform under different operating conditions. The proposed configuration could be very useful for modern load centers where on-site PV generation and strict voltage regulation are required.

References

[1] R. A. Walling, R. Saint, R. C. Dugan, J. Burke, and L. A. Kojovic, "Summary of distributed resources impact on power delivery systems," *IEEE Trans. Power Del.*, vol. 23, no. 3, pp. 1636–1644, Jul. 2008.

[2] C. Meza, J. J. Negroni, D. Biel, and F. Guinjoan, "Energy-balance modeling and discrete control for single-phase grid-connected PV central inverters," *IEEE Trans. Ind. Electron.*, vol. 55, no. 7, pp. 2734–2743, Jul. 2008.

[3] T. Shimizu, O. Hashimoto, and G. Kimura, "A novel high-performance utility-interactive photovoltaic inverter system," *IEEE Trans. Power Electron.*, vol. 18, no. 2, pp. 704–711, Mar. 2003.

[4] S. B. Kjaer, J. K. Pedersen, and F. Blaabjerg, "A review of single-phase grid-connected inverters for photovoltaic modules," *IEEE Trans. Ind. Appl.*, vol. 41, no. 5, pp. 1292–1306, Sep./Oct. 2005.

[5] T. Esram, J. W. Kimball, P. T. Krein, P. L. Chapman, and P. Midya, "Dynamic maximum power point tracking of photovoltaic arrays using ripple correlation control," *IEEE Trans. Power Electron.*, vol. 21, no. 5, pp. 1282–1291, Sep. 2006.

[6] *IEEE Recommended Practices and Requirements for Harmonic Control in Electrical Power Systems*, IEEE Standard 519-1992, Apr. 1993, pp. 1–112.

[7] J. A. Martinez and J. M. Arnedo, "Voltage sag studies in distribution networks—Part I: System modeling," *IEEE Trans. Power Del.*, vol. 21, no. 3, pp. 338–345, Jul. 2006.

[8] J. D. Li, S. S. Choi, and D. M. Vilathgamuwa, "Impact of voltage phase jump on loads and its mitigation," in *Proc. 4th Int. Power Electron. Motion Control Conf.*, Xian, China, Aug. 14–16, 2004, vol. 3, pp. 1762–1766.

[9] S. S. Choi, J. D. Li, and D. M. Vilathgamuwa, "A generalized voltage compensation strategy for mitigating the impacts of voltage sags/swells," *IEEE Trans. Power Del.*, vol. 20, no. 3, pp. 2289–2297, Jul. 2005.

[10] Y. W. Li, D. M. Vilathgamuwa, F. Blaabjerg, and P. C. Loh, "A robust control scheme for medium-voltage-level DVR implementation," *IEEE Trans. Ind. Electron.*, vol. 54, no. 4, pp. 2249–2261, Aug. 2007.

[11] H. K. Al-Hadidi, A. M. Gole, and D. A. Jacobson, "Minimum power operation of cascade inverter-based dynamic voltage restorer," *IEEE Trans. Power Del.*, vol. 23, no. 2, pp. 889–898, Apr. 2008.

[12] J. Kaniewski, Z. Fedyczak, and G. Benysek, "AC voltage sag/swell compensator based on three-phase hybrid transformer with buck-boost matrix-reactance chopper," *IEEE Trans. Ind. Electron.*, vol. 61, no. 8, pp. 3835–3846, Aug. 2014.

[13] J. G. Nielsen and F. Blaabjerg, "A detailed comparison of system topologies for dynamic voltage restorers," *IEEE Trans. Ind. Appl.*, vol. 41, no. 5, pp. 1272–1280, Sep./Oct. 2005.

[14] C. Liu, B. Wu, N. R. Zargari, D. Xu, and J. Wang, "A novel three-phase three-leg ac/ac converter using nine IGBTs," *IEEE Trans. Power Electron.*, vol. 24, no. 5, pp. 1151–1160, May 2009.

[15] T. Kominami and Y. Fujimoto, "A novel three-phase inverter for independent control of two three-phase loads," in *Proc. IEEE Ind. Appl. Soc. (IAS)*, 2007, pp. 2346–2350.

[16] T. Kominami and Y. Fujimoto, "Inverter with reduced switching-device count for independent AC motor control," in *Proc. 33rd Annu. Conf. IEEE Ind. Electron. Soc. (IECON'07)*, 2007, pp. 1559–1564.

[17] C. Liu, B. Wu, N. R. Zargari, and D. Xu, "A novel nine-switch PWM rectifier-inverter topology for three-phase UPS applications," in *Proc. IEEE Everyday Pract. Electron. (EPE)*, 2007, pp. 1–10.

[18] L. Zhang, P. C. Loh, and F. Gao, "An integrated nine-switch power conditioner for power quality enhancement and voltage sag mitigation," *IEEE Trans. Power Electron.*, vol. 27, no. 3, pp. 1177–1190, Mar. 2011.

[19] M. Azizi, A. Fatemi, M. Mohamadian, and A. Y. Varjani, "Integrated solution for microgrid power quality assurance," *IEEE Trans. Energy Convers.*, vol. 27, no. 4, pp. 992–1001, Dec. 2012.

[20] P. Kanjiya, B. Ambati, and V. Khadkikar, "A novel fault-tolerant DFIG-based wind energy conversion system for seamless operation during grid faults," *IEEE Trans. Power Syst.*, vol. 29, no. 3, pp. 1296–1305, May 2014.

[21] *IEEE P1547 Standard for Distributed Resources Interconnected With Electric Power Systems*, IEEE Standard P1547, Sep. 2002.

Abdul Mannan Rauf received the B.Sc. degree from the University of Engineering and Technology, Taxila, Pakistan, in 2009, and the M.Sc. degree in electrical engineering from Masdar Institute of Science and Technology, Abu Dhabi, UAE, in 2014.

Since August 2014, he has been a Research Engineer with Masdar Institute of Science and Technology. His research interests include power electronics, power quality enhancement, and grid integration of inverter-based renewable energy systems.

Vinod Khadkikar (S'06–M'09) received the B.E. degree from the Government College of Engineering, Dr. Babasaheb Ambedkar Marathwada University, Aurangabad, India, in 2000, the M. Tech. degree from the Indian Institute of Technology (IITD), New Delhi, India, in 2002, and the Ph.D. degree from the École de Technologie Supérieure (E.T.S.), Montréal, QC, Canada, in 2008, all in electrical engineering.

From December 2008 to March 2010, he was a Postdoctoral Fellow with the University of Western Ontario, London, ON, Canada. From April 2010 to December 2010, he was a Visiting Faculty with Massachusetts Institute of Technology, Cambridge, MA, USA. Currently, he is an Associate Professor with Masdar Institute of Science and Technology, Abu Dhabi, UAE. His research interests include applications of power electronics in distribution systems and renewable energy resources, grid interconnection issues, power quality enhancement, active power filters, and electric vehicles.

Dr. Khadkikar is currently an Associate Editor of the *IET Power Electronics Journal*.